Academic Journal of Science and Technology
ISSN: 2771-3032 | Vol. 15, No. 2, 2025

Preparation and Properties of $CsPbX_3$(X=Br, I) Quantum Dots

Yingjie Wen, Hari Bala*, Yunpeng Zhao

Henan Polytechnic University, Jiaozuo, China
* Corresponding author

Abstract: The all-inorganic perovskite quantum dot $CsPbX_3$ (X = Cl, Br, I) exhibits unique optical properties enabled by its bandgap tunability. $CsPbX_3$ quantum dots with varying I^- doping ratios were synthesized via ligand-assisted reprecipitation (LARP). Appropriate I^- doping can effectively modulate the lattice parameters of the quantum dots, resulting in a redshift of the absorption band edge and a narrowing of the optical band gap in the ultraviolet-visible absorption spectrum. Excessive I^- doping induces a 91% reduction in fluorescence quantum yield due to lattice distortion. Transmission electron microscopy (TEM) and X-ray diffraction (XRD) analyses confirmed that the quantum dot size was highly uniform and the monoclinic crystal phase remained stable. Ultraviolet-visible diffuse reflection spectroscopy and fluorescence spectroscopy elucidated the synergistic effects of quantum confinement and exciton recombination dynamics. This study underscores the significant impact of I^- doping on Br-based perovskites, providing a foundation for the rational design of heterojunctions in perovskite systems.

Keywords: All-inorganic perovskite quantum dots; I^- doping modulation; Optical bandgap narrowing; Lattice distortion.

1. Introduction

In recent years, all-inorganic perovskite materials have demonstrated significant potential in the field of photocatalysis owing to their exceptional photoelectric performance. For example, these materials exhibit high photoluminescence quantum yield[1,2] (PLQY), narrow full width half maximum[3,4] (FWHM), and tunable emission spectra[5,6]. These remarkable characteristics render them promising candidate materials for applications in light-emitting diodes[7] (LEDs), high-definition flexible displays, solar cells[8,9], and other optoelectronic devices.

For $CsPbX_3$ quantum dots, as the radius of the halogen atoms increases ($Cl^- < Br^- < I^-$), the lattice constant also increases, while the critical temperature for the cubic-to-tetragonal phase transition decreases. By precisely tuning the Cl/Br/I ratio, the fluorescence emission range of $CsPbX_3$ quantum dots can be extended from the ultraviolet region (~410 nm, Cl-based) to the near-infrared region (~760 nm, I-based). Zhu et al. elaborated in detail that halogen modification of $CsPbX_3$ (X = Cl, Br, I) quantum dots can achieve full-spectrum tunable luminescence[10]. Furthermore, they elucidated the intrinsic mechanisms underlying the quantum confinement effect and exciton recombination in these quantum dots. Although research on perovskite quantum dots has advanced rapidly, the effects resulting from halogen hybridization warrant further in-depth investigation.

The liquid-phase chemical synthesis of perovskite quantum dots has led to the development of several well-established methods, including thermal injection[11,12] (HI), ligand-assisted reprecipitation[13] (LARP), microwave-assisted synthesis[14], and solvent-thermal approaches[15]. Each method exhibits distinct advantages in terms of process characteristics and application scenarios. Currently, the hot injection method is widely regarded as the optimal approach for synthesizing quantum dots with greater homogeneity and superior performance. Nevertheless, research into solutions that are more cost-effective and energy-efficient remains valuable. Sun et al. successfully synthesized perovskite quantum dots at room temperature via the LARP method, facilitated by the use of medium and short-chain ligands[16]. Li et al. developed monoclinic CsPbX3 all-inorganic perovskite quantum dots at room temperature through a comparable rate-controlled recrystallization approach, further demonstrating the feasibility of low-temperature synthesis for high-quality quantum dots[13]. Compared with Cl-based and I-based quantum dots, Br-based materials demonstrate superior environmental stability attributed to their moderate lattice energy and defect formation energy. Specifically, the ionic radius of Cl^- is smaller, resulting in higher Pb-Cl bond energy, a tighter lattice structure, and better thermal stability compared to the Br^- and I^- systems. Nevertheless, halogen vacancy defects on its surface can lead to a decrease in photoluminescence (PL) intensity as temperature increases. Additionally, the ultraviolet light absorption range of Cl^- is not ideal for optoelectronic research. The relatively large ionic radius of I^- causes the Goldschmidt tolerance factor (t value) to deviate from the ideal range (0.8–1.0)[17], leading to a tendency for the cubic phase to transform into a regular intersecting phase. Additionally, the bond energy of the Pb-I bond is relatively low, making it susceptible to phase transformation and decomposition in polar solvents or oxygen-rich environments. The ionic radius of Br^- and the bond energy of Pb-Br lie between those of Cl^- and I^-, resulting in moderate lattice stability and high PL efficiency (up to 95%).

Herein, based on bromide Br-based perovskites, this study investigates the synthesis of $CsPbX_3$ quantum dots with enhanced performance by finely tuning the ratio of halogen ions Br and I. This approach ensures an optimal balance between superior light absorption intensity and material stability. The qualitative analysis of the synthesized quantum dots was performed using transmission electron microscopy (TEM) and X-ray diffraction (XRD) to evaluate the specific effects of ion doping. Furthermore, the light absorption intensity and photoluminescence properties of the obtained samples were systematically characterized using a UV-Vis spectrophotometer and a fluorescence spectrometer. A

comprehensive discussion on the influence of ion doping on the overall performance of the quantum dots is also presented.

2. Experimental

2.1. Chemicals and reagents

Oleic acid (OA, 98%), oleylamine (OAm, 90%), N, N-dimethylformamide (DMF, ACS), cesium bromide (CsBr, 99.9%), lead bromide ($PbBr_2$, 99.9%), cesium iodide (CsI, 99.9%) and lead iodide (PbI_2, 99.9%) were all purchased from Macklin.

2.2. Synthesis of $CsPb(Br_{1-x}I_x)_3$ Perovskite Quantum Dots

$CsPb(Br_{1-x}I_x)_3$ perovskite quantum dots were synthesized by adapting previously reported methods with minor modifications. Specifically, an equimolar amount (0.4 mmol) of CsX_2 and PbX_2 was dissolved in 5 mL of DMF. Subsequently, a mixture of oleic acid and oleylamine, maintained at a fixed volume ratio of 2:1, was added to the solution after ensuring complete dissolution of the solutes. The precursor solution was then prepared through thorough stirring for 30 minutes at room temperature. Finally, the precursor solution was slowly injected into a vigorously stirred toluene solution, resulting in the immediate formation of a $CsPb(Br_{1-x}I_x)_3$ quantum dot solution exhibiting strong fluorescence emission.

2.3. Characterizations

The micromorphology of the samples was characterized using a high-resolution transmission electron microscope (HRTEM; FEI Talos F200S, USA). Elemental distribution was analyzed via energy dispersive X-ray spectroscopy (EDS) coupled with a scanning electron microscope (SEM; Merlin Compact, Germany). X-ray diffraction (XRD) patterns were recorded under Cu Kα radiation using a X-ray diffractometer (Smart Lab 9 kW, Rigaku, Japan). Time-resolved photoluminescence (TRPL) spectra were obtained under 400 nm excitation with a steady-state/transient fluorescence spectrometer (Edinburgh FLS1000, UK), and steady-state photoluminescence (PL) spectra were also acquired. UV-Vis diffuse reflectance spectra (DRS) were measured using a UV-Vis spectrophotometer (UV-6100S, China) with BaSO4 as the reference material. The light absorption properties of the solution were evaluated using another UV-Vis spectrophotometer (TU-1810PCS, China).

3. Results and Discussion

3.1. Sample Appearance

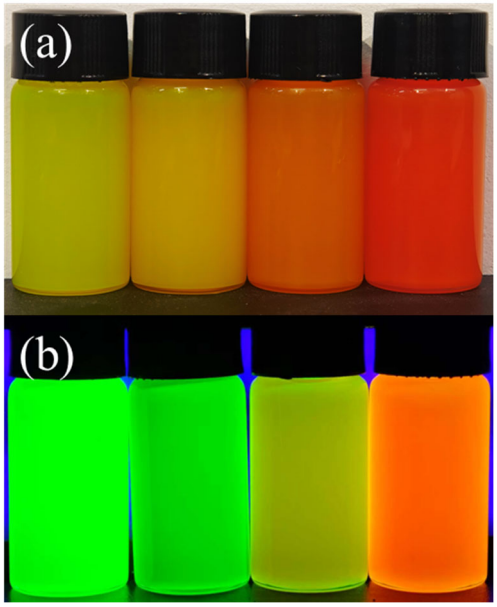

Figure. 1. Images of $CsPbX_3$ quantum dot suspensions synthesized under varying I^- doping concentrations are presented under (a) natural light and (b) ultraviolet light. The samples, arranged from left to right, correspond to doping levels of 10%, 20%, 30%, and 40%, respectively.

The synthesis of quantum dots via LARP was characterized by its rapidity and pronounced reaction phenomena. The changes in the quantum dots under natural light and ultraviolet (UV) irradiation can be directly observed. As shown in Figure 1(a) and (b), photographs depict $CsPbX_3$ (X = Br, I) quantum dots with varying I^- doping concentrations prepared under both natural light and UV illumination. The respective doping proportions of I^- were set at 10%, 20%, 30%, and 40%. From these images, it is evident that the synthesized quantum dots exhibit homogeneity and relative stability. With increasing I^- doping concentration, a noticeable color variation is observed. Furthermore, UV lamp irradiation results indicate that varying I^- ratios cause the fluorescence emission of the quantum dots to progressively shift toward the red region of the spectrum. However, the fluorescence intensity, or fluorescence quantum yield, decreases gradually with increasing I^- content. These observations align well with the synthetic principles governing halide differentiation in all-inorganic perovskites and corroborate the findings reported by Li et al[13]. Therefore, when synthesizing $CsPbX_3$ quantum dots using the LARP method, the incorporation of I^- significantly influences the stability and optical properties of the quantum dots.

3.2. TEM and microscopic morphology analysis

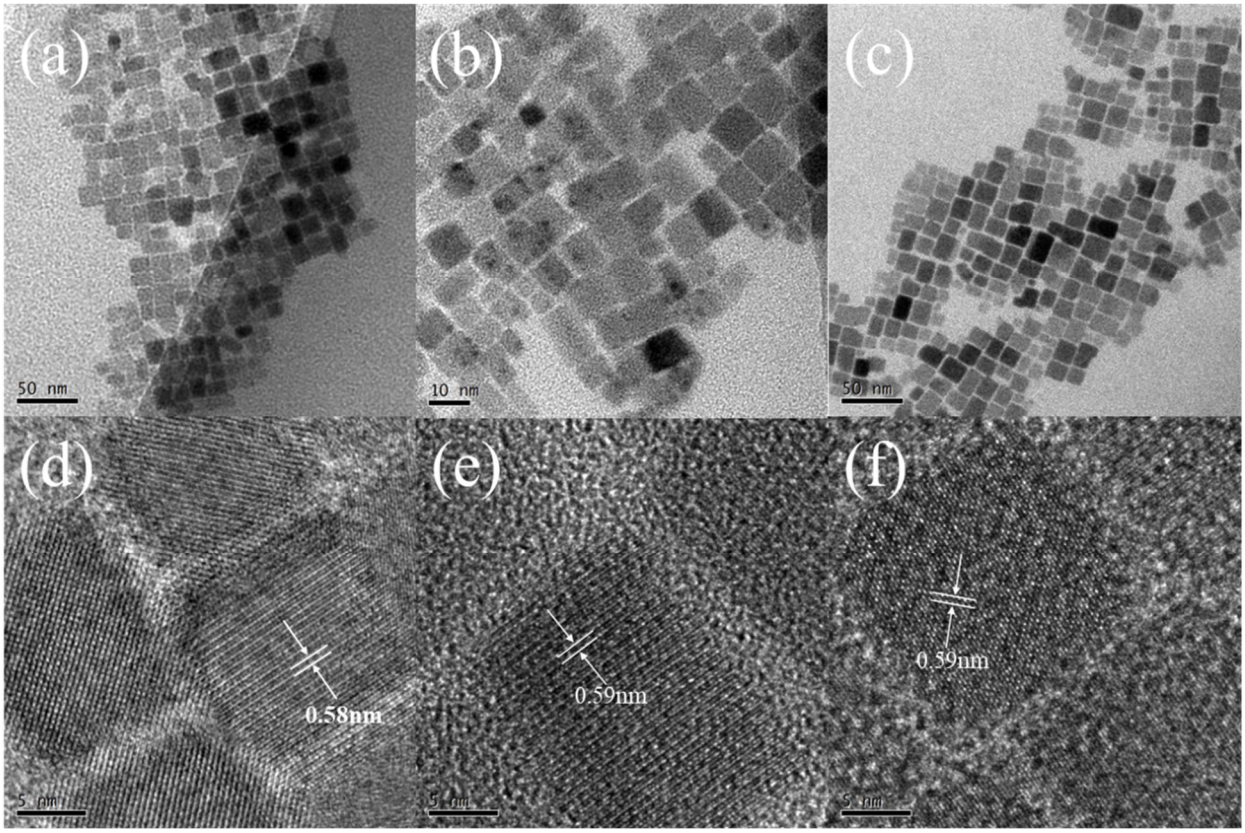

Figure. 2. TEM images of (a) $CsPbBr_3$, (b) $CsPb(Br_{0.8}I_{0.2})_3$, and (c)$CsPb(Br_{0.6}I0._4)_3$ quantum dots HRTEM images of (d)$CsPbBr_3$, (e)$CsPb(Br_{0.8}I_{0.2})_3$ and (f)$CsPb(Br_{0.6}I_{0.4})_3$ quantum dots

To investigate the influence of I^- doping on the morphology and lattice spacing of $CsPbX_3$ (X = Br, I) quantum dots, their microscopic structures were analyzed using transmission electron microscopy (TEM). As depicted in Figure. 2, the samples correspond to $CsPbBr_3$, $CsPb(Br_{0.8}I_{0.2})_3$, and $CsPb(Br_{0.6}I0_{0.4})_3$, respectively. From Figure. 2(a)-(c), it is evident that as the concentration of I^- increases continuously, the uniformity of $CsPbX_3$ quantum dots deteriorates, while the average particle size gradually increases to approximately 10-15 nm with good crystallinity. This phenomenon can be attributed to the lattice expansion induced by the larger ionic radius of I^-. By examining the high-resolution TEM (HRTEM) images shown in Figure. 2(d)-(f), it is observed that the perovskite lattice remains almost unchanged. The interplanar spacings for $CsPbBr_3$, $CsPb(Br_{0.8}I_{0.2})_3$, and $CsPb(Br_{0.6}I0_{0.4})_3$ are 0.58 nm, 0.59 nm, and 0.59 nm, respectively. Based on the standard crystal plane spacing of 0.58 nm for $CsPbBr_3$, these spacings are identified as corresponding to the (110) crystal planes. With the continuous increase in I^- concentration, the lattice spacing exhibits a slight increase, consistent with the behavior of halide ions in $CsPbX_3$ quantum dots. However, given the relatively low atomic numbers of halogens (Cl, Br, I; e.g., Cl = 17, Br = 35, I = 53), traditional bright-field/dark-field TEM imaging struggles to directly resolve their atomic positions or doping distributions. Additionally, as the I^- concentration continues to rise, phase transformations may occur. Therefore, the optimal doping ratio must be determined in conjunction with optical properties. Nonetheless, it is confirmed that low concentrations of I^- doping have minimal effects on the lattice size of $CsPbX_3$ (X = Br, I) quantum dots and do not induce significant lattice distortion.

To further confirm the successful incorporation of I^- into $CsPbX_3$ quantum dots, scanning electron microscopy (SEM) and energy-dispersive X-ray spectroscopy (EDS) were employed for elemental analysis. Figure 3(a) presents the SEM image of $CsPbX_3$ (X = Br, I) quantum dots, while Figures 3(b), (c), (d), and (e) depict the elemental distribution maps of Cs, Pb, Br, and I, respectively. Based on the scale of the transmission electron microscopy (TEM) image, the $CsPbX_3$ quantum dots are identified as nanocrystals that aggregate into bulk structures at the micrometer scale. By analyzing the elemental distribution in Figures 3(b)-(e), it is evident that Cs, Pb, Br, and I are present, with a reasonable distribution pattern. The unique $[PbX_6]^{4-}$ structure of $CsPbX_3$ quantum dots facilitates the enrichment of halogen ions on the surface of the quantum dots, which aligns with the observed elemental distribution. The limited yet distinct distribution of I^- further confirms its incorporation into the quantum dot lattice.

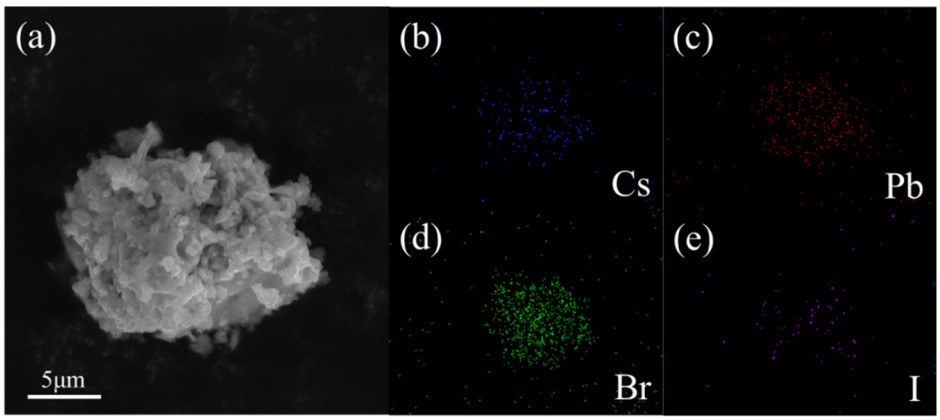

Figure. 3. (a) SEM images of $CsPbX_3$(X=Br, I) quantum dots; EDS element distribution maps of $CsPbX_3$(X=Br, I) quantum dots: (b)Cs, (c)Pb, (d)Br and (e)I

3.3. XRD analysis

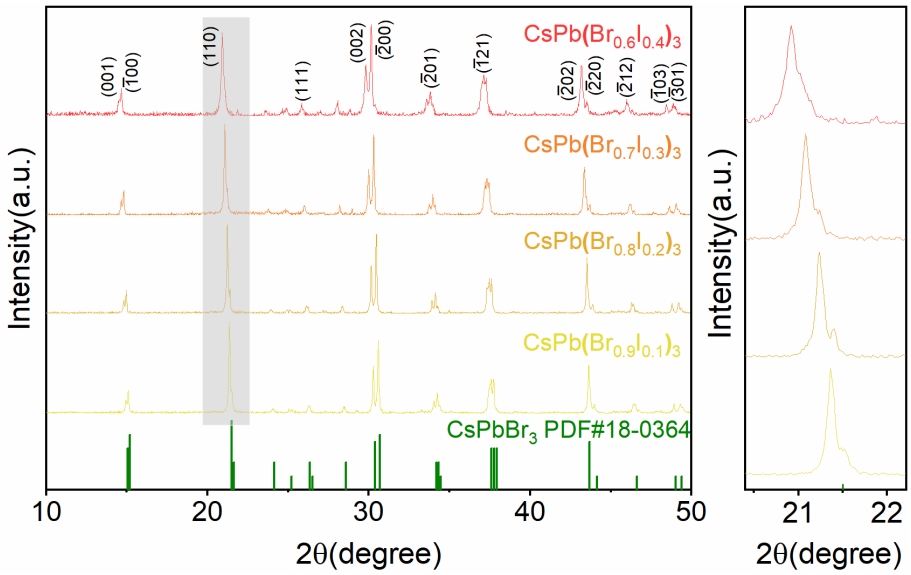

Figure 4. XRD patterns of $CsPbX_3$ (X = Br, I) quantum dots doped with varying concentrations of I^- ions.

To systematically investigate the influence of I^- doping on the crystal structure of $CsPbX_3$ (X = Br, I) quantum dots, X-ray diffraction (XRD) analyses were performed on samples with I^- concentrations of 10%, 20%, 30%, and 40%, respectively. As shown in Figure 3-4, the lattice diffraction peaks of all $CsPbX_3$ (X = Br, I) quantum dots align with the characteristic peaks of $CsPbBr_3$ quantum dots and belong to the monoclinic phase (JCPDS No. 18-0364). The diffraction peaks of $CsPbBr_3$ quantum dots are observed at 2θ = 15.1°, 15.2°, 21.5°, 26.3°, 30.4°, 30.7°, 34.3°, 37.8°, 43.7°, 44.1°, 46.6°, 49.0°, and 49.4°, corresponding to the crystal planes (001), ($\bar{1}$00), (110), (111), (002), ($\bar{2}$00), ($\bar{2}$01), ($\bar{1}$21), ($\bar{2}$02), ($\bar{2}$20), ($\bar{2}$12), ($\bar{1}$03), and ($\bar{3}$01), respectively. However, the prepared $CsPbX_3$ (X = Br, I) quantum dots do not perfectly match the lattice diffraction peaks of $CsPbBr_3$ quantum dots. Instead, as the concentration of I^- increases gradually, the lattice shifts toward smaller angles, consistent with the Bragg equation: $n\lambda = 2d\sin\theta$. Specifically, an increase in the interplanar spacing d results in a decrease in the lattice diffraction peak angle 2θ, indicating an inverse relationship between the two. Despite the incorporation of I^-, the shift in diffraction peaks suggests that no derivative phase was formed due to I^- intercalation, indirectly confirming the sufficient lattice stability of the synthesized $CsPbX_3$ quantum dots. Based on the tristrong peak principle, the peaks at 2θ = 15.1°, 21.5°, and 30.7° correspond to the (001), (110), and ($\bar{2}$00) planes, respectively, indicating relatively high purity of the prepared $CsPbX_3$ quantum dots. Furthermore, under conditions where the lattice structure of $CsPbX_3$ quantum dots remains unchanged, I^- combines with Br^- to form highly pure $CsPbX_3$ quantum dots.

3.4. Analysis of Optical Properties

To systematically investigate the influence of varying I^- doping ratios on the optical properties of $CsPbX_3$ (X = Br, I) quantum dots, a UV-Vis spectrophotometer was employed to measure the UV-Vis absorption spectra of a series of colloidal solutions with different I^- doping concentrations. The results are presented in Figure 5. As shown in Figure 5, it is evident that as the I^- doping ratio increases gradually, the absorption spectrum of $CsPbX_3$ quantum dots exhibits a redshift, and the light absorption band edge expands from 520 nm to 580 nm. Each sample effectively covers the lower-energy region of the absorption spectrum, demonstrating the excellent visible-light absorption capability of $CsPbX_3$ quantum dots. Notably, while a higher I^- doping ratio broadens the light absorption band edge, normalization analysis reveals that the light absorption intensity of $CsPbX_3$ quantum dots prepared under identical conditions is somewhat compromised. This phenomenon indirectly suggests that excessive I^- doping

introduces surface defects, which may create deep energy-level traps and promote non-radiative recombination, thereby reducing the overall light absorption efficiency. Conversely, an appropriate amount of I^- doping can fill Br^- vacancies, reduce the density of defect states, and enhance the absorption intensity. Thus, I^- doping serves as an effective means to modulate the light absorption range of quantum dots, offering enhanced versatility for their applications in diverse optoelectronic devices.

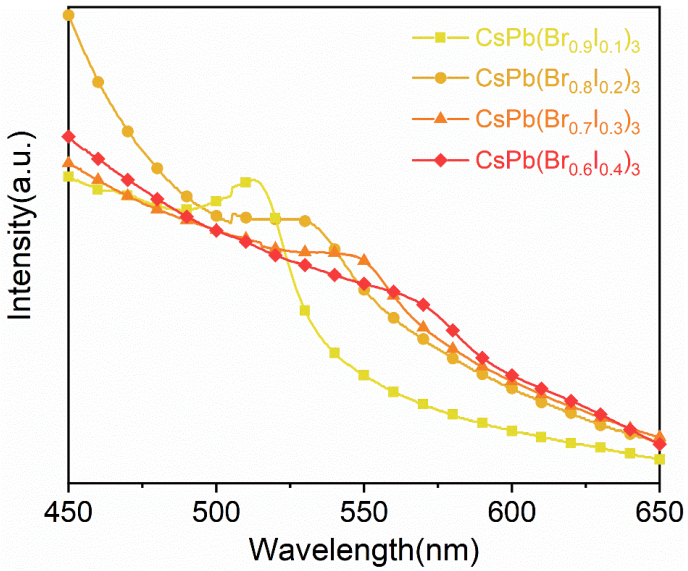

Figure. 5. Ultraviolet-Visible Absorption Spectra of $CsPbX_3$ (X = Br, I) Quantum Dots Doped with I^- Ions at Various Concentrations

In addition to observing the redshift of the absorption spectrum, attention should also be directed toward the variations in exciton absorption peaks[18]. In the investigation of the optical properties of quantum dots, the concept of exciton absorption peaks is highly significant. Excitons are quasiparticles formed through Coulomb interactions between electrons and holes. In all-inorganic perovskites $CsPbX_3$ (X = Br, I), the incorporation of I^- may result in a broader size distribution of quantum dots. This phenomenon can be likened to introducing small spheres of varying sizes (owing to the size difference between I^- and Br^-) into a group of initially uniform spheres (originally relatively homogeneous quantum dots), thereby causing disorder in the overall size distribution. Such changes in size distribution influence the state of excitons, as the dimensions of quantum dots are closely associated with exciton properties. Furthermore, the introduction of I^- may induce lattice distortion. The lattice, originally a regular periodic structure akin to a neatly arranged square array, becomes disrupted upon the insertion of irregular elements (I^- ions). This distortion affects exciton generation. The cumulative effect of these two factors leads to an increase in the half-peak width of the exciton absorption peak in the ultraviolet-visible absorption spectrum. As shown in Figure 5, the exciton absorption peaks correspond to the inflection points of the lines in the ultraviolet-visible absorption spectrum, specifically the "bulges" at wavelengths of 514 nm, 533 nm, 550 nm, and 570 nm. The half-peak width can be determined by observing the change in radians. An increase in the half-peak width signifies an expansion of the spectral response range, enabling quantum dots to absorb visible light across a broader wavelength range compared to their previous narrower response.

The band structure plays a pivotal role in electron transitions and energy transfer within semiconductor materials. Under standard conditions, $CsPbBr_3$ quantum dots exhibit a specific band gap. The reorganization of the band structure induced by I^- doping leads to a reduction in the band gap. When I^- is doped into $CsPbBr_3$ quantum dots, the disparity in ionic radii significantly affects the crystal lattice structure due to the relatively large ionic radius of I^-. Upon incorporation into the quantum dot lattice, I^- induces lattice expansion. This expansion is not merely a physical size change but also triggers the reorganization of the energy band structure within the crystal. In crystalline structures, electron energy states are discretely distributed across different energy bands, with band gaps separating these energy bands. Changes in the lattice structure result in corresponding adjustments to the electron energy states, thereby altering the band gap. From the perspective of light absorption, the reduction in the band gap manifests as a shift of the light absorption edge toward longer wavelengths, corresponding to the redshift phenomenon observed in the ultraviolet-visible (UV-Vis) absorption spectrum. As depicted in Figure 6, the band gap (E_g) of the prepared materials is calculated using the Kubelka-Munk equation. It can be inferred from Figure 6 that the optical band gaps of $CsPb(Br_{0.9}I_{0.1})_3$, $CsPb(Br_{0.8}I_{0.2})_3$, $CsPb(Br_{0.7}I_{0.3})_3$, and $CsPb(Br_{0.6}I_{0.4})_3$ are 2.26 eV, 2.15 eV, 2.13 eV, and 2.05 eV, respectively. With increasing I^- doping ratios, more I^- ions enter the lattice structure of the quantum dots, enhancing lattice expansion and energy band structure reorganization, which further reduces the band gap. This implies enhanced absorption capacity for long-wavelength light, offering significant potential for optical applications[19].

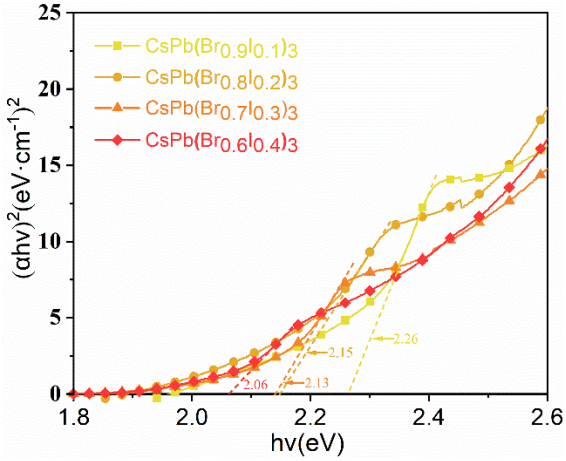

Figure. 6. band gap calculation curves for $CsPbX_3$ (X = Br, I) quantum dots doped with I^- ions at varying concentrations.

In the synthesis of all-inorganic perovskite $CsPbX_3$ (X = Br, I), I^- doping substantially alters its photoluminescence (PL) spectral characteristics and influences fluorescence stability. To investigate this effect, PL spectroscopy measurements were performed on $CsPbX_3$ quantum dots with varying I^- doping ratios, as illustrated in Figure 7(a). The incorporation of I^- induces a narrowing of the band gap in $CsPbX_3$, leading to a redshift in the PL emission peak position. Through halide exchange ($Br^- \rightarrow I^-$), I^- doping modulates the fluorescence spectral peak positions of the quantum dots, promoting the migration of emission peaks from the green light region (approximately 520 nm) toward the red-light region (approximately 610 nm), thereby enabling controllable spectral tuning. Additionally, I^- doping can induce lattice distortion or non-uniform size distribution, resulting in an increase in the full width at half maximum of the fluorescence peak from 18 nm to 28 nm. This redshift in the fluorescence peak position correlates with that observed in the ultraviolet-visible absorption spectrum. Furthermore, the temporal decay of fluorescence intensity was examined for $CsPbX_3$ quantum dots doped with different I^- ratios. The larger ionic radius of I^- may introduce lattice strain, increase surface defect density, and compromise long-term stability. As depicted in Figures 7(b)-(d), it is evident that at a 40% I^- doping level, the rate of fluorescence intensity decay is significantly faster compared to samples with lower I^- doping levels. After 36 hours, the fluorescence attenuation rates were measured as 61% for $CsPbBr_3$ quantum dots, 77% for $CsPb(Br_{0.8}I_{0.2})_3$ quantum dots, and 91% for $CsPb(Br_{0.6}I_{0.4})_3$ quantum dots. As shown in Figure 7(d), excessive I^- doping leads to high surface defect densities, accelerating quantum dot decomposition, opening octahedral voids in defect regions, and causing significant structural degradation.

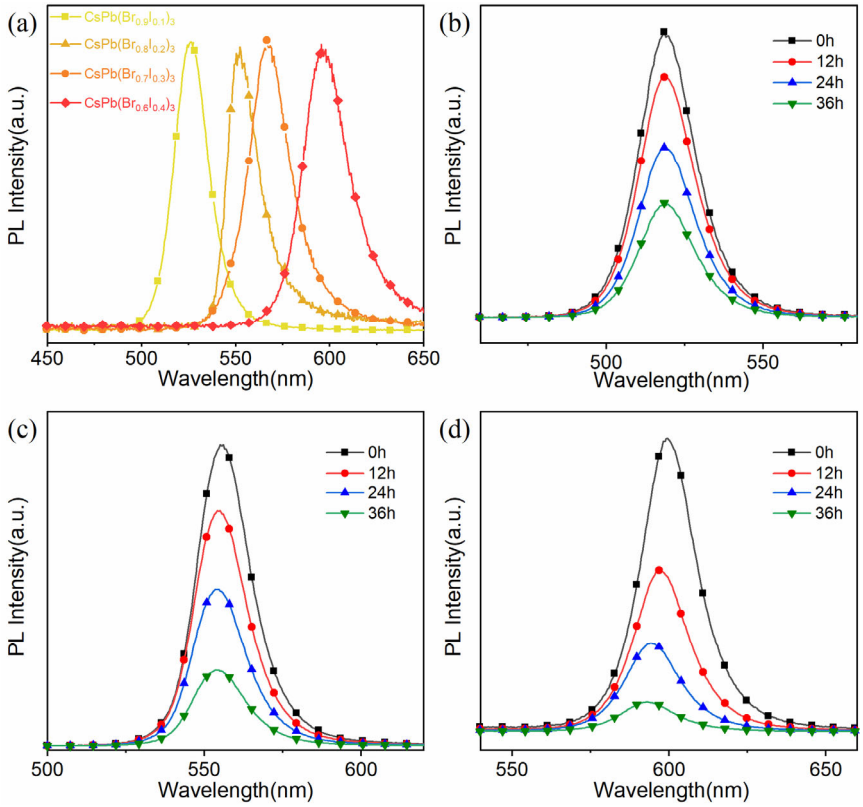

Figure. 7. (a) PL fluorescence spectra of $CsPbX_3$ (X = Br, I) quantum dots doped with varying concentrations of I^- ions, (b) fluorescence spectra of $CsPbBr_3$ quantum dots, (c) $CsPb(Br_{0.8}I_{0.2})_3$ quantum dots, and (d) $CsPb(Br_{0.6}I_{0.4})_3$ quantum dots monitored over time.

4. Conclusions

In conclusion, the impact of I^- doping on the morphology, lattice characteristics, and optical properties of $CsPbX_3$ quantum dots, using $CsPbBr_3$ as the substrate, was systematically investigated via ligand-assisted reprecipitation. The findings indicate that the size of the quantum dots exhibits a slight increase with the rising proportion of I^-, while a low level of I^- doping does not compromise the lattice structure of $CsPbX_3$ quantum dots. Furthermore, I^- doping induces a tendency for the diffraction peaks of crystal planes to shift towards smaller angles. Optical analysis was employed to explore the influence of the I^- ratio on the absorption band edge and bandgap of $CsPbX_3$ quantum dots. When the I^- doping concentration reaches 20%, the quantum dots demonstrate optimal optical performance and stability, providing an ideal foundation for subsequent design and protection strategies for $CsPbX_3$ quantum dots.

References

[1] Chun F, Jang K Y, Zhou H, et al. Ultrasmall 2D Sn-Doped MAPbBr3 Nanoplatelets Enable Bright Pure-Blue Emission[J]. Small, 2024: 2400959.

[2] Zhao G G, Zhang M, Li H X, et al. Velocity field distribution control in antisolvent flow realizing highly stable and efficient perovskite nanocrystals[J]. Journal of Colloid and Interface Science, 2023, 649: 214-222.

[3] Zhang M, Zhang J Y, Gu L, et al. Ultranarrow Deep-Blue Luminescence of Perovskite Nanocrystals by A-Site Cation Control[J]. Acs Applied Materials & Interfaces, 2024, 16(24): 31524-31533.

[4] Zhang X Y, Wang Q Q, Yao Z W, et al. Stable Perovskite Quantum Dots Light-Emitting Diodes with Efficiency Exceeding 24%[J]. Advanced Science, 2023, 10(36): 2304696.

[5] Zhang X B, Wu X D, Xu Y H, et al. Tailoring Fe3+-Activated Broadband NIR Phosphors: Enhancing External Quantum Efficiency and Spectrum Adjustability Through Crystal Field Engineering in Double Perovskite Antimonate Structures[J]. Advanced Optical Materials, 2024, 12(10): 2302300.

[6] Yang C, Fan C L, Hussain F, et al. Luminescent ionic lattice occupation and wide tunable emission spectra of La2MgZrO6:Bi3+,Eu3+ double perovskite phosphors for white light LED[J]. Journal of Rare Earths, 2023, 41(4): 489-497.

[7] Li X W, Cai W S,Guan H L, et al. Highly stable CsPbBr3 quantum dots by silica-coating and ligand modification for white light-emitting diodes and visible light communication[J]. Chemical Engineering Journal, 2021, 419: 129551.

[8] Nuket P, Akaishi Y, Yoshimura G, et al. In-situ TiO2-Coated CsPbBr3 quantum dots with enhanced stability, photoluminescence quantum yields, and charge transport properties[J]. Ceramics International, 2022, 48(21): 32504-32512.

[9] Wen Z R, Liang C, Li S W, et al. High-Quality van der Waals Epitaxial CsPbBr3 Film Grown on Monolayer Graphene Covered TiO2 for High-Performance Solar Cells[J]. Energy & Environmental Materials, 2024, 7(4): e12680.

[10] Ullah S, Wang J, Yang P, et al. All-inorganic CsPbBr3 perovskite: a promising choice for photovoltaics[J]. Materials Advances, 2021, 2(2): 646-683.

[11] Murray C B, Norris D J, Bawendi M G. Synthesis and characterization of nearly monodisperse CdE (E = sulfur, selenium, tellurium) semiconductor nanocrystallites[J]. Journal of the American Chemical Society, 1993, 115(19): 8706-8715.

[12] Protesescu L, Yakunin S, Bodnarchuk M I, et al. Nanocrystals of Cesium Lead Halide Perovskites (CsPbX3, X = Cl, Br, and I): Novel Optoelectronic Materials Showing Bright Emission with Wide Color Gamut[J]. Nano Letters, 2015, 15(6): 3692-3696.

[13] Li X, Wu Y, Zhang S, et al. CsPbX3 Quantum Dots for Lighting and Displays: Room-Temperature Synthesis, Photoluminescence Superiorities, Underlying Origins and White Light-Emitting Diodes[J]. Advanced Functional Materials, 2016, 26(15): 2435-2445.

[14] Tong Y, Bladt E, Aygüler M F, et al. Highly Luminescent Cesium Lead Halide Perovskite Nanocrystals with Tunable Composition and Thickness by Ultrasonication[J]. Angewandte Chemie International Edition, 2016, 55(44): 13887-13892.

[15] Chen M, Zou Y, Wu L, et al. Solvothermal Synthesis of High-Quality All-Inorganic Cesium Lead Halide Perovskite Nanocrystals: From Nanocube to Ultrathin Nanowire[J]. Advanced Functional Materials, 2017, 27(23): 1701121.

[16] Protesescu, L, Yakunin, S, Bodnarchuk, M I, et al. Nanocrystals of Cesium Lead Halide Perovskites (CsPbX3, X = Cl, Br, and I): Novel Optoelectronic Materials Showing Bright Emission with Wide Color Gamut[J]. 2015, 15(6): 3692-3696.

[17] Bartel C J, Sutton C, Goldsmith B R, et al. New tolerance factor to predict the stability of perovskite oxides and halides[J]. Science Advances, 2019, 5(2): eaav0693.

[18] Wu Y, Wei H, Xu L, et al. Progress and perspective on CsPbX3 nanocrystals for light emitting diodes and solar cells[J]. Journal of Applied Physics, 2020, 128(5): 050903.

[19] Kong L, Zhang X, Zhang C, et al. Stability of Perovskite Light-Emitting Diodes: Existing Issues and Mitigation Strategies Related to Both Material and Device Aspects[J]. Advanced Materials, 2022, 34(43): 2205217.